

# Graphene-gold/PDMS Maxwell hybrid nanofluidic flow in a squeezed channel with linear and irregular radiations

Dhanekula Naga Bhargavi<sup>1</sup>, Kotha Gangadhar<sup>2</sup>   
and Ali J. Chamkha<sup>3</sup>

Proc IMechE Part E:

J Process Mechanical Engineering

2024, Vol. 238(1) 203–212

© IMechE 2022

Article reuse guidelines:

sagepub.com/journals-permissions

DOI: 10.1177/09544089221139696

journals.sagepub.com/home/pie



## Abstract

The hydrothermal performance of a hybrid nanofluid made of graphene, gold/polydimethylsiloxane between two squeezing plates is discussed in this study. In the investigation of thermal transport of the flow, both linear and nonlinear thermal radiation's effects are taken into account. Bejan numbers are used to determine the system's energy efficiency. Viscous and thermal radiation effects on Maxwell hybrid nanofluid flow in a squeezing channel are incorporated to explore the outcomes. By applying similarity transformations, the set of ordinary differential equations in this case is transformed into the governing equations. With the use of the Runge–Kutta–Fehlberg technique converted system is solved numerically. Skin friction and heat transfer rates under the influence of certain oriented parameters are numerically analysed and presented in tabular form. The impacts of different factors on the temperature and velocity profiles are illustrated graphically and briefly described. Important findings include that the Bejan number raises as the radiation parameter  $R_d$  rises, but that it falls with respect to the Eckert number effect. Additionally, the skin friction values and Nusselt number in the hybrid nanofluid case are larger than in the nanofluid case. Furthermore, it has been found that the Deborah number-described stress relaxation phenomenon causes the flow field and thermal energy transfer to be less efficient when fluids are moving. There is surprisingly little research on the hybrid fluid integrated into their issues.

## Keywords

Hybrid nanofluid, graphene, gold, squeezing channel, nonlinear radiation, PDMS fluid

Date received: 2 October 2022; accepted: 1 November 2022

## 1. Introduction

As we know that most of the mechanical devices function with the usual movement of the piston, for example, it can be seen on the inside of the automobile's engine. The actual example of clutching movement is the piston and two plates' motion in an engine. Additional examples include fluid flow, hydraulic crane pistons, engine operation, and electronic motors. As all we know, the functioning of the human heart is to pump blood through squeezing to all parts of the body. Because of this importance in real life, the squeezed flow among two parallel surfaces is the greatest fascinating field in the research of fluid dynamics as well as it took an equally important role in the biological sciences field also. The most suitable examples of squeezing movement are the flow of fluid in syringes and a nasogastric tube.

The fundamental understanding of the squeezed flow was proposed by Stefan.<sup>1</sup> Through the HAM, Siddiqui et al.<sup>2</sup> investigated the two-dimensional squeeze flow between two surfaces. Hayat et al.<sup>3</sup> examined various situations of heat transfer at the time of squeeze flow

via two parallel plates. For more information about the squeezed flow in different geometry can be found in Vajravelu et al.,<sup>4</sup> Khan et al.,<sup>5</sup> and Mustafa et al.<sup>6</sup> Bejan<sup>7</sup> offered a creative solution to reduce the entropy production in the convective heat transfer phenomenon. Entropy creation is, in essence, a measurement of the unpredictability of the molecules created in a thermodynamic system. The second law of thermodynamics states that the quality of energy degrades as molecular chaos does. Began<sup>8</sup> emphasised that energy dissipation and heat transfer resulting from temperature differences

<sup>1</sup>Department of Mathematics, Vignan's Nirula Institute of Technology and Science for Women, Palakaluru, Guntur, Andhra Pradesh, India

<sup>2</sup>Department of Mathematics, Acharya Nagarjuna University, Ongole Campus, Andhra Pradesh, India

<sup>3</sup>Faculty of Engineering, Kuwait College of Science and Engineering, Doha District, Kuwait

### Corresponding author:

Kotha Gangadhar, Department of Mathematics, Acharya Nagarjuna University, Ongole Campus, Andhra Pradesh-523001, India.

Email: kgangadharmaths@gmail.com

are the primary drivers for entropy production. The second law was then examined by a number of researchers using a variety of geometries and physical conditions. Gul et al.<sup>9</sup> described how mixed convection effects the generation of entropy in the Poiseuille flow of Jeffery nanofluid using perturbation technique. The effects of thermal radiation, viscosity dissipation, and entropy creation on Maxwell nanofluid through a squeezing channel were studied recently by Shit and Mukherjee<sup>10</sup> using the differential transformation approach. They came to the conclusion that when Deborah increases, the heat transmission rate decreases. In addition to all these mentioned studies, some researchers have reported regarding the studies of entropy generation in Marzougui et al.,<sup>11</sup> Sarbazi and Hormozi,<sup>12</sup> Mehta et al.,<sup>13</sup> Abbasi et al.,<sup>14</sup> and Zheng et al.<sup>15</sup>

In the present trend, a serious scientific investigation is going on into the composite of graphene-polymer. It is involved in the applications of science and engineering.<sup>16</sup> Ground-breaking research in this area has demonstrated that graphene-silicon nanoparticles (G-putty) are sensitive electromechanical sensors that can also detect spider foot-falls. The thermophysical characteristics of the hybrid graphene-gold/polydimethylsiloxane (PDMS) nanofluid have attracted a lot of attention in recent years. Choi and Eastman<sup>17</sup> initially coined the term “nanofluid” to describe fluids containing suspended nanoparticles ( $10^{-9}$  nm), which are more commonly known as nanoparticles. The industry uses the special properties of nanofluids, which have higher thermal conductivity with less nanoparticle aggregation, strong temperature dependence of thermal conductivity, and nonlinear increase in thermal conductivities, for cooling nuclear reactions, extracting geothermal energy, producing car fuels, and cooling radiators. Furthermore, it is more beneficial for engineering applications like electronic device cooling, smart fluids, and the biological and pharmaceutical industries. Numerous researchers have contributed to the debate on nanofluid flow across various geometries as a result of the aforementioned applications.<sup>18–24</sup>

On the flip side, a mixture of two distinct types of nanoparticles dispersed in a base fluid is referred to as a hybrid nanofluid. Such kind of fluids develops the heat capacity of the base fluid. Basically, hybrid nanofluids are having the capacity to smoothly flow through micro-cavities along with their dispersing properties. Hybrid nanoparticles can achieve good thermal conductivity due to improved convection between them and the base fluid. The major benefits of including nanoparticles to base fluid are to enhance heat transmission, effective surface area, collisions, capacity of strong heat, and interaction between the nanoparticles. Because of such importance, esteemed researchers<sup>25–42</sup> concluded that from their observations fluid heat capacity can be improved by single and hybrid nano-additives.

These research works have considerably motivated us to investigate the characteristics of the flow of graphene-gold/PDMS hybrid Maxwell nanofluid among two parallel squeezing plates. Entropy generation is used to assess

energy efficiency. Also, impacts of viscous dissipation and nonlinear radiations as well as the nanoparticles volume fraction are investigated thoroughly. The originality of the current examination is the entropy generation of the hybrid nanofluid taking into account both linear and nonlinear radiation effects. The proposed examination has significant applications in injection modelling, polymer processing, and so on. By adjusting various factors used in the current investigation, Bejan number and Nusselt number are evaluated in depth. Additionally studied are the velocity, temperature, and skin friction coefficient profiles.

## 2. Modelling of the problem

This study examined the flow of viscid and incompressible hybrid nanofluid of graphene-gold-PDMS in a compressible channel and studied widely about the features of heat transfer and entropy generation. This content is illustrated by the 2-D Cartesian coordinate system, in which the coordinate  $\xi_1$  contains plates and coordinate  $\xi_2$  shows the direction of the normal to the plates as illustrated in Figure 1. The distance among the two parallel plates at time  $t$  is  $h(t) = H(1 - \gamma t)^{1/2}$  (measured from  $\xi_2 = 0$ ). Here,  $\gamma > 0$  stands for the speed and direction of the plates. The rate of speed of the plates is  $v(t) = dh/dt$ , and they ultimately collide at time  $t = 1/\gamma$ . The  $\gamma < 0$  values show that plates are far apart. Initially, at time  $t = 0$ , the distance among the plates is  $H$ . In our system, the linear and nonlinear radiative heat flux is considered in our system.

The thermophysical characteristics of the base fluid, nanofluid and hybrid nanofluid are presented in Table 1. These considerations along with boundary-layer approximations and governing equations for the flow are as follows:

$$\vec{\nabla} \cdot \vec{V} = 0, \quad (1)$$

$$\rho_{hnf} \left( \frac{\partial \vec{V}}{\partial t} \right) + (\vec{V} \cdot \vec{\nabla}) \vec{V} = -\vec{\nabla} p + \mu_{hnf} \nabla^2 \vec{V} + \vec{\nabla} \cdot \mathcal{S}, \quad (2)$$

$$\begin{aligned} (\rho C_p)_{hnf} \left( \left( \frac{\partial \vec{T}}{\partial t} \right) + (\vec{V} \cdot \vec{\nabla}) \vec{T} \right) \\ = \vec{\nabla} \cdot (k \vec{\nabla} \cdot \vec{T}) + \vec{\nabla} q_r + \Phi, \end{aligned} \quad (3)$$

In Equation (2),  $\mathcal{S}$  is the extra stress tensor for upper-convected Maxwell fluid, which satisfies the following:

$$\mathcal{S} + \lambda_1 \frac{D\mathcal{S}}{Dt} = \mu A_1, \quad (4)$$

where  $\lambda_1$  is the fluid relaxation time,  $A_1 = (\vec{\nabla} \cdot \vec{V}) + (\vec{\nabla} \cdot \vec{V})'$  the first Rivlin–Ericksen tensor, and  $D/Dt$  the upper-convected time derivative. Invoking the conventional boundary-layer approximations, equations (1) to

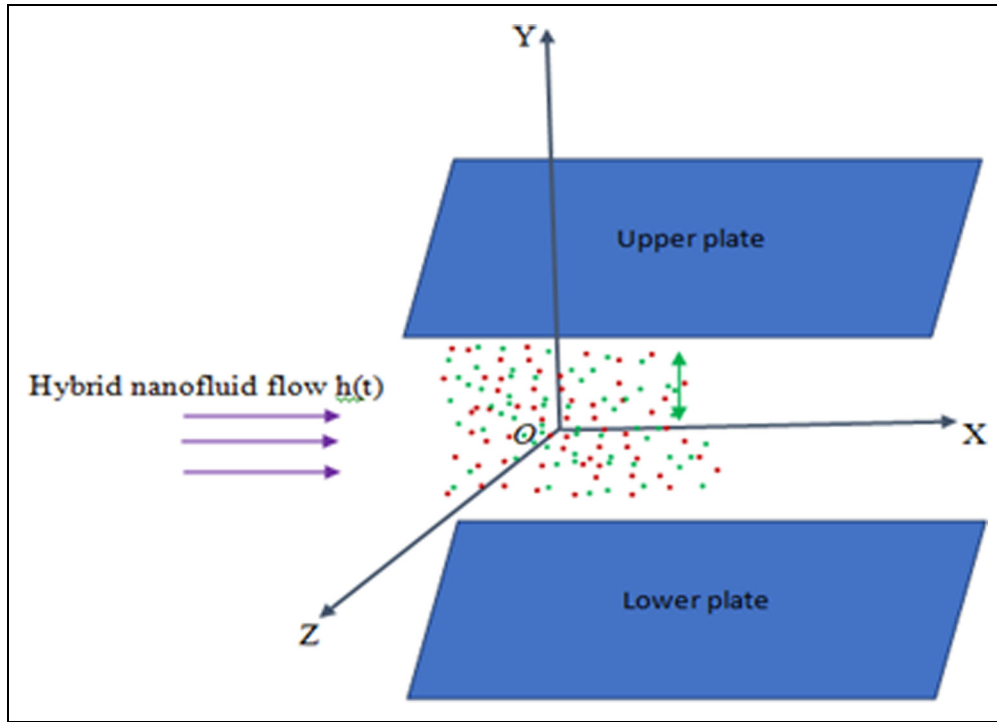


Figure 1. Physical sketch of the problem.

Table 1. Thermophysical properties of the base fluid, nanofluids, and hybrid nanofluid<sup>10</sup>

	$\rho$ [kg m <sup>-3</sup> ]	$C_p$ [J kg <sup>-1</sup> K <sup>-1</sup> ]	$k$ [Wm <sup>-1</sup> K <sup>-1</sup> ]
PDMS fluid	816	2000	0.15
Gold	19300	129	318
Graphene	2250	710	3000

(3) can be expressed in component forms<sup>10</sup> as follows:

$$\frac{\partial f_1}{\partial \xi_1} + \frac{\partial f_2}{\partial \xi_2} = 0, \tag{5}$$

$$\begin{aligned} \rho_{hnf} \left( \frac{\partial f_1}{\partial t} + f_1 \frac{\partial f_1}{\partial \xi_1} + f_2 \frac{\partial f_1}{\partial \xi_2} \right) &= - \frac{\partial p}{\partial \xi_1} \\ - \rho_{hnf} \lambda_1 \left( f_1^2 \frac{\partial^2 f_1}{\partial \xi_1^2} + f_2^2 \frac{\partial^2 f_1}{\partial \xi_2^2} + 2f_1 f_2 \frac{\partial^2 f_1}{\partial \xi_1 \partial \xi_2} \right) \\ + \mu_{hnf} \left( \frac{\partial^2 f_1}{\partial \xi_1^2} + \frac{\partial^2 f_1}{\partial \xi_2^2} \right), \end{aligned} \tag{6}$$

$$\begin{aligned} \rho_{hnf} \left( \frac{\partial f_2}{\partial t} + f_1 \frac{\partial f_2}{\partial \xi_1} + f_2 \frac{\partial f_2}{\partial \xi_2} \right) &= - \frac{\partial p}{\partial \xi_2} \\ - \rho_{hnf} \lambda_1 \left( f_1^2 \frac{\partial^2 f_2}{\partial \xi_1^2} + f_2^2 \frac{\partial^2 f_2}{\partial \xi_2^2} + 2f_1 f_2 \frac{\partial^2 f_2}{\partial \xi_1 \partial \xi_2} \right) \\ + \mu_{hnf} \left( \frac{\partial^2 f_2}{\partial \xi_1^2} + \frac{\partial^2 f_2}{\partial \xi_2^2} \right), \end{aligned} \tag{7}$$

$$\begin{aligned} \frac{\partial T}{\partial t} + f_1 \frac{\partial T}{\partial \xi_1} + f_2 \frac{\partial T}{\partial \xi_2} &= \frac{\kappa_{hnf}}{(\rho c_p)_{hnf}} \left( \frac{\partial^2 T}{\partial \xi_1^2} + \frac{\partial^2 T}{\partial \xi_2^2} \right) \\ - \frac{1}{(\rho c_p)_{hnf}} \frac{\partial q_r}{\partial \xi_2} + \frac{\mu_{hnf}}{(\rho c_p)_{hnf}} \\ \left( 2 \left( \left( \frac{\partial f_1}{\partial \xi_1} \right)^2 + \left( \frac{\partial f_2}{\partial \xi_2} \right)^2 \right) + \left( \frac{\partial f_1}{\partial \xi_2} + \frac{\partial f_2}{\partial \xi_1} \right)^2 \right), \end{aligned} \tag{8}$$

where  $f_1$  and  $f_2$  signifies the components in the direction of  $\xi_1$  and  $\xi_2$  axis, correspondingly. The radiative heat flux is estimated by considering Rosseland estimation, as

$$q_r = - \frac{4\sigma_0}{3k_0} \frac{\partial T^4}{\partial \xi_2} = - \frac{16\sigma_0}{3k_0} T^3 \frac{\partial T}{\partial \xi_2}, \tag{9}$$

where  $\sigma_0$ ,  $k_0$  are, respectively, the Stefan–Boltzmann constant and mean absorption coefficients. The very high non-linear energy equation in  $T$  is produced by Equation (9), and it is highly tough to get the solution. Although, in earlier, the researchers evaluated this problem by guessing minor temperature differences within the flow (see Gangadhar et al.<sup>22</sup>). Under these circumstances, the Rosseland formula can be linearised over ambient temperature  $T_H$ . It just means replacing  $T^3$  in Equation (9) with  $T_H^3$ . Now (8) can be expressed as follows:

$$\begin{aligned} \frac{\partial T}{\partial t} + f_1 \frac{\partial T}{\partial \xi_1} + f_2 \frac{\partial T}{\partial \xi_2} &= \frac{\kappa_{hnf}}{(\rho c_p)_{hnf}} \left( \frac{\partial^2 T}{\partial \xi_1^2} + \frac{\partial^2 T}{\partial \xi_2^2} \right) \\ + \frac{1}{(\rho c_p)_{hnf}} \frac{16\sigma_0 T_H^3}{3k_0} \frac{\partial^2 T}{\partial \xi_2^2} + \frac{\mu_{hnf}}{(\rho c_p)_{hnf}} \\ \left( 2 \left( \left( \frac{\partial f_1}{\partial \xi_1} \right)^2 + \left( \frac{\partial f_2}{\partial \xi_2} \right)^2 \right) + \left( \frac{\partial f_1}{\partial \xi_2} + \frac{\partial f_2}{\partial \xi_1} \right)^2 \right), \end{aligned} \tag{10}$$

Although the assumption which is stated earlier is avoided, the radiative heat flow in Equation (8) produces a very high nonlinear expression of radiation that is the subject of the present research. Therefore, the energy equation for the flow of nonlinear thermal radiation will be as follows:

$$\begin{aligned} \frac{\partial T}{\partial t} + f_1 \frac{\partial T}{\partial \xi_1} + f_2 \frac{\partial T}{\partial \xi_2} &= \frac{\kappa_{hnf}}{(\rho c_p)_{hnf}} \left( \frac{\partial^2 T}{\partial \xi_1^2} + \frac{\partial^2 T}{\partial \xi_2^2} \right) \\ &+ \frac{1}{(\rho c_p)_{hnf}} \frac{\partial}{\partial \xi_2} \left( \frac{16\sigma_0 T^3}{3k_0} \frac{\partial T}{\partial \xi_2} \right) + \frac{\mu_{hnf}}{(\rho c_p)_{hnf}} \\ &\left( 2 \left( \left( \frac{\partial f_1}{\partial \xi_1} \right)^2 + \left( \frac{\partial f_2}{\partial \xi_2} \right)^2 \right) + \left( \frac{\partial f_1}{\partial \xi_2} + \frac{\partial f_2}{\partial \xi_1} \right)^2 \right). \end{aligned} \quad (11)$$

### 2.1. Effective density

$\rho_{nf}$  is the effective density of the convectational nanoliquid and is defined by<sup>20</sup>

$$\rho_{nf} = (1 - \phi)\rho_{bf} + \phi\rho_s, \quad (12)$$

Here,  $\phi$  denotes solid volume fraction, and  $\rho$  denotes density, whereas the subscripts “bf, s” indicate, respectively, base fluid and solid nanoparticles, so the effective density ( $\rho_{hnf}$ ) of hybrid nanoliquid is given by<sup>21</sup>

$$\rho_{hnf} = (1 - \phi_2)\{(1 - \phi_1)\rho_f + \phi_1\rho_{s1}\} + \phi_2\rho_{s2} \quad (13)$$

where  $\phi_1, \phi_2$  are solid volume fractions of gold and graphene nanoparticles, and  $\rho_{s1}$  and  $\rho_{s2}$  are densities of gold and graphene, respectively.

### 2.2. Effective heat capacity

Regular nanoliquid’s effective heat capacity is determined by<sup>20</sup>

$$(\rho c_p)_{nf} = \phi(\rho c_p)_s + (1 - \phi)(\rho c_p)_{bf} \quad (14)$$

The effective heat capacitance expression of hybrid nanoliquid ( $(\rho c_p)_{hnf}$ ) has the following form<sup>21</sup>:

$$\begin{aligned} (\rho c_p)_{hnf} &= (1 - \phi_2)\{\phi_1(\rho c_p)_{s1} + (1 - \phi_1)(\rho c_p)_f\} \\ &+ \phi_2(\rho c_p)_{s2} \end{aligned} \quad (15)$$

### 2.3. Effective thermal conductivity

Based on the Maxwell–Garnetts model,<sup>20</sup>  $k_{nf}$  is the thermal conductivity of typical nanofluid and is given by

$$k_{nf} = \frac{(k_s + 2k_{bf}) - 2\phi(k_{bf} - k_s)}{(k_s + 2k_{bf}) + \phi(k_{bf} - k_s)} k_{bf}, \quad (16)$$

Hence, the thermal conductivity of hybrid nanofluid contains spherical nanoparticles<sup>21</sup> described as

$$k_{hnf} = \frac{(k_{s2} + 2k_{nf}) - 2\phi_2(k_{nf} - k_{s2})}{(k_{s2} + 2k_{nf}) + \phi_2(k_{nf} - k_{s2})} k_{bf}, \quad (17)$$

### 2.4. Effective dynamic viscosity

$\mu$  is the effective dynamic viscosity, the subscripts “nf” and “hnf” correspond to regular nanofluid and hybrid nanofluid based on the Brinkman model<sup>20,21</sup> are accordingly given by

$$\mu_{nf} = \frac{\mu_{bf}}{(1 - \phi)^{2.5}}, \quad (18)$$

$$\mu_{hnf} = \frac{\mu_{bf}}{(1 - \phi_1)^{2.5}(1 - \phi_2)^{2.5}}, \quad (19)$$

The boundary conditions are considered as

$$f_1 = 0, \quad f_2 = \frac{dh}{dt}, \quad T = T_H \text{ at } \xi_2 = h(t) \quad (20)$$

$$\frac{\partial f_1}{\partial \xi_2} = 0, \quad f_2 = 0, \quad \frac{\partial T}{\partial \xi_2} = 0 \text{ at } \xi_2 = 0 \quad (21)$$

The subsequent parallel alterations and non-dimensional variables are presented<sup>10</sup>:

$$\begin{aligned} \eta &= \frac{\xi_2}{H\sqrt{1 - \gamma t}}, \quad f_1 = \frac{\gamma \xi_1}{2(1 - \gamma t)} F'(\eta), \\ f_2 &= \frac{-\gamma H}{2\sqrt{1 - \gamma t}}, \quad G = \frac{T - T_H}{T_w - T_H}, \end{aligned} \quad (22)$$

with  $T = T_H(1 + (\theta_w - 1)G)$  and  $\theta_w = \frac{T_w}{T_H}$  (temperature ratio parameter with  $T_w > T_H$ ). Using these non-dimensional variables and removing the pressure terms by means of the mutual derivatives (6) and (7), the resulting ordinary non-linear differential equations are derived together with the thermal equations (10) and (11) as follows:

$$\begin{aligned} F^{iv} &= Sq A_1 (1 - \phi_1)^{2.5} (1 - \phi_2)^{2.5} \\ &\left( 3F'' + \eta F'''' + F'F'' - FF'''' \right. \\ &\left. - \frac{De}{2} (F''F'^2 - 3FF'F'''' + FF''^2 - 2F^2F^{iv}) \right), \end{aligned} \quad (23)$$

$$\begin{aligned} &\left( 1 + \frac{4}{3} Rd \right) G'' + Pr Sq \frac{A_2}{A_3} (FG' - \eta G') \\ &+ \frac{Pr Ec}{A_3 (1 - \phi_1)^{2.5} (1 - \phi_2)^{2.5}} (F'^2 + 4\delta^2 F'^2) \\ &= 0, \end{aligned} \quad (24)$$

$$\begin{aligned} &\left[ \left( 1 + \frac{4}{3} Rd(1 + (\theta_w - 1)G) \right) G' \right]' + Pr Sq \frac{A_2}{A_3} (FG' - \eta G') \\ &+ \frac{Pr Ec}{A_3 (1 - \phi_1)^{2.5} (1 - \phi_2)^{2.5}} (F'^2 + 4\delta^2 F'^2) = 0, \end{aligned} \quad (25)$$

Likewise, the boundary conditions (21) and (22) reduce to

$$F''(0) = 0, F(0) = 0, G'(0) = 0, \quad (26)$$

$$F'(1) = 0, F(1) = 1, G(1) = 1, \quad (27)$$

Equations (19) to (21) contain some dimensional parameters determined as the squeezing number  $Sq = \frac{\gamma H^2}{2\nu_f}$ ,  $A_1 = \frac{\rho_{mf}}{\rho_f}$ ,

$$A_2 = \frac{(\rho c_p)_{mf}}{(\rho c_p)_f}, A_3 = \frac{k_{mf}}{k_f}, \quad \text{the Eckert number}$$

$$Ec = \frac{\rho_f}{(\rho c_p)_f T_H} \left( \frac{ax}{2(1-\gamma t)} \right)^2, \quad \text{the Prandtl number}$$

$$Pr = \frac{\mu_f (\rho c_p)_f}{\rho_f k_f}, \quad \text{the Deborah number}$$

$$De = \frac{\gamma \lambda_1}{1-\gamma t} \delta = \frac{H \sqrt{1-\gamma t}}{x}, \quad \text{and the thermal radiation}$$

$$\text{parameter } Rd = \frac{4\sigma_0 T_H^3}{k_0 k_f}.$$

In this article, we investigate the skin friction coefficient  $C_f$  and the Nusselt number  $Nu$  which can be stated as

$$C_f = \frac{\mu_{mf} \left( \frac{\partial f_1}{\partial \xi_2} \right)_{\xi_2=h(t)}}{\frac{1}{2} \rho_{mf} \left( \frac{dh}{dt} \right)^2} = \frac{2F''(1)}{Sq \delta A_1 (1-\phi_1)^{2.5} (1-\phi_2)^{2.5}}, \quad (28)$$

$$Nu = \frac{-H k_{mf} \left( \frac{\partial T}{\partial \xi_2} \right)_{\xi_2=h(t)}}{k_f T_H} = \frac{-Nu_r}{\sqrt{1-\gamma t}}, \quad (29)$$

where  $Nu_r = -A_3 G'(1)$ .

### 3. Entropy generation

Here, entropy generation is caused due to the irreversible loss of thermal energy in the system. The main goal of the modern research is to achieve the maximum efficiency of any mechanical system by reducing entropy. It can be accomplished by the variations of physical parameters included in the present analysis. Now, the rate of entropy generation per unit volume is given below according to the author<sup>10</sup>:

$$S_{Total} = \frac{k_{mf}}{k_f} \left( \left( \frac{\partial T}{\partial \xi_2} \right)^2 + \frac{16\sigma_0 T_H^3}{3k_0 k_{mf}} \left( \frac{\partial T}{\partial \xi_2} \right)^2 \right) + \frac{\mu_{mf}}{T} \left( \frac{\partial f_1}{\partial \xi_2} \right)^2 \quad (30)$$

$$S_{Total} = \frac{k_{mf}}{k_f} \left( \left( \frac{\partial T}{\partial \xi_2} \right)^2 + \frac{16\sigma_0 T^3}{3k_0 k_{mf}} \left( \frac{\partial T}{\partial \xi_2} \right)^2 \right) + \frac{\mu_{mf}}{T} \left( \frac{\partial f_1}{\partial \xi_2} \right)^2 \quad (31)$$

Here in Equation (30) involved linear radiation and in Equation (31) involved nonlinear radiation term.

The non-dimensional form for the total entropy generation is as follows:

$$Es = \frac{h(t)^2}{k_{mf}} S_{Total} = E_{ST} + E_{SFF} = \frac{1}{G^2} \left( 1 + \frac{4}{3} Rd \right) G'^2 + \frac{1}{G A_3 (1-\phi_1)^{2.5} (1-\phi_2)^{2.5}} F'^2, \quad (32)$$

$$Es = \frac{h(t)^2}{k_{mf}} S_{Total} = E_{ST} + E_{SFF} = G'^2 (\theta_w - 1)^2 \left[ \frac{4}{3} Rd (G(\theta_w - 1) + 1) + \frac{1}{(G(\theta_w - 1) + 1)^2} \right] + \frac{1}{(G(\theta_w - 1) + 1) A_3 (1-\phi_1)^{2.5} (1-\phi_2)^{2.5}} F'^2, \quad (33)$$

where the entropy generation due to the thermal effects is represented by  $E_{ST}$  and the entropy generation of the fluid friction is  $E_{SFF}$ . The linear radiation Equation (32), non-linear radiation Equation (33) shows the contribution to the entropy generation. Compare the contributions graphically and identify the factor which provides more in the total entropy generation. For this reason, a very significant dimensionless number, that is, the Bejan number  $Be$  which helps us to compare the factors  $E_{ST}$  to the  $E_s$ . The Bejan number formula is as follows:

$$Be = \frac{E_{ST}}{E_s}. \quad (34)$$

### 4. Method of solution

Equations (23) to (25) are a set of coupled nonlinear differential equations together with the boundary conditions (26) and (27) and are evaluated numerically with the help of shooting technique and fourth- to fifth-order R–K–F integration scheme jointly by altering it into an initial value problem. In this process, it is essential to select an appropriate finite value of  $\eta \rightarrow \infty$ , say  $\eta_\infty$ , that is,  $\eta_\infty = 1$ . We design succeeding the first-order system.

$$t'_1 = t_2, \quad t'_2 = t_3, \quad t'_3 = t_4, \quad (35)$$

$$[1 + 2 Sq A_1 (1-\phi_1)^{2.5} (1-\phi_2)^{2.5}] t'_4 = Sq A_1 (1-\phi_1)^{2.5} (1-\phi_2)^{2.5} \left[ 3t_3 + \eta t_4 + t_2 t_3 - t_1 t_4 - \frac{De}{2} (t_3 t_2^2 - 3t_1 t_2 t_4 + t_1 t_3^2) \right], \quad (36)$$

$$t'_5 = t_6, \quad (37)$$

**Table 2.** Comparison of present numerical data and previously published data.

$Pr$	$Ec$	$-\theta'(0)$ Zheng et al. <sup>15</sup>	$-\theta'(0)$ Pournmehrhan et al. <sup>19</sup>	$-\theta'(0)$ Acharya et al. <sup>18</sup>	$-\theta'(0)$ Shit and Mukherjee <sup>10</sup>	$-\theta'(0)$ Present results
0.5	1.0	1.5222368	1.518859607	1.5222367498	1.52237	1.5223675888175043
1.0	1.0	3.0263240	3.019545607	3.0263235590	3.02633	3.0263245025929186
2.0	1.0	5.9805300	5.967887511	5.9805303980	5.98053	5.98053186244505
5.0	1.0	14.4394100	14.413946780	14.4394132400	14.43940	14.439416999446689
1.0	0.5	1.5131620	1.509772834	1.5131618070	1.51316	1.51316193156508
1.0	1.2	3.6315880	3.623454726	3.6315882690	3.63160	3.6315893011003273
1.0	2.0	6.0526470	6.039091204	6.0526471080	6.05266	6.052648433997164
1.0	5.0	15.1316200	15.097728080	15.1316178400	15.13160	15.131619967282623

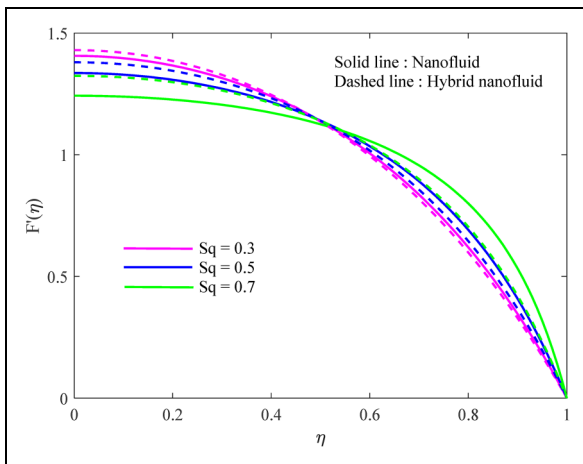


**Figure 2.** Velocity versus  $Sq$  for both nanofluid and hybrid nanofluid when  $De = 0.5$ ,  $\delta = 0.1$ ,  $Rd = 0.2$ ,  $Pr = 6.2$ ,  $\theta_w = 2$ , and  $Ec = 0.1$ .

$$\left[ 1 + \frac{4}{3}Rd(1 + (\theta_w - 1)t_5)^3 \right] t_6' = -4Rd$$

$$(1 + (\theta_w - 1)t_5)^2 t_6^2 (\theta_w - 1)$$

$$- Pr Sq \frac{A_2}{A_3} (t_1 t_6 - \eta t_6) - \frac{Pr Ec}{A_3(1 - \phi_1)^{2.5}(1 - \phi_2)^{2.5}}$$

$$(t_3^2 + 4\delta^2 t_2^2), \tag{38}$$

Boundary conditions are

$$t_3(0) = 0, \quad t_1(0) = 0, \quad t_6(0) = 0, \tag{39}$$

$$t_2(1) = 0, \quad t_1(1) = 1, \quad t_5(1) = 1. \tag{40}$$

To solve equations (23) to (25) along with boundary conditions (26) and (27), the values for  $t_3(0)$ , that is,  $F''(0)$ ,  $t_5(0)$ , that is,  $G'(0)$  are required but these values are not provided here. Initially, estimate the values for  $F''(0)$  and  $G'(0)$  and then use the R–K integration technique of the fourth to fifth order to achieve the solution. Then at  $\eta\infty$  the resulting values of  $F'(\eta)$  and  $G(\eta)$  are compared to the existing boundary conditions  $F'(1) = 1$  and

$G(1) = 1$  and by using the shooting technique adjust the values of  $F''(0)$  and  $G'(0)$  to contribute better estimations for the solution. Repeated the process till the desired accuracy of results is achieved, correct up to level  $10^{-9}$ , which meets the convergence criterion. Table 2 describes the conformation of the present outcomes by comparing with the existing literature for certain limited special cases.<sup>6,10,15,18,19</sup> The comparison shows an intelligent agreement for all  $Pr$  and  $Ec$  values, confirming the validity of current results. For numerical outcomes, we considered the values of dimensionless parameters as  $\phi_1 = 0.1$ ,  $\phi_2 = 0.1$ ,  $Sq = 0.5$ ,  $De = 0.5$ ,  $\delta = 0.1$ ,  $Rd = 0.2$ ,  $Pr = 6.2$ ,  $\theta_w = 2$ , and  $Ec = 0.1$ . These values remain valid throughout the study except for the modifications in related figures and tables.

### 5. Results and discussions

The main goal of this section is to examine the effects of several examination-related parameters, including the radiation parameter, Eckert number, Deborah number, volume fractions of nanoparticles, and squeezing parameter. Hence, Figures 2 to 9 have been plotted for such an objective. Figures 2 to 4 detail the relationship between changes in the axial velocity in the direction of  $\xi_2$  and the changes in the squeezing parameter  $Sq$ , the  $De$  number and the solid volume fraction of nanoparticles  $\phi_2$ . In fact, squeezing parameter  $Sq$  illustrates the speed of the parallel plates which are movable relative to each other (or away when  $Sq$  is chosen as a negative value) and  $De$  number can calculate the proportion of the relaxation time to observation time. From Figure 2, it might be seen that velocity diminishes at the middle region and then the opposite trend is clearly visible near the channel wall for the increase of squeezing parameter  $Sq$ . Figure 3 displays that as  $De$  number increases to a certain height, the velocity component tends to decrease and after that reverse trend continues. Physically, when the Deborah number  $De$  increases, the stress relaxation phenomenon in viscoelastic fluid increases and the liquid becomes more solid-like for the fluid motion and slows down. According to Figure 4, the velocity increases initially and achieves maximum value as the volume fraction of solid increases, thereafter we can observe a reduction with increasing  $\eta$  even though  $\phi_2$  increases.

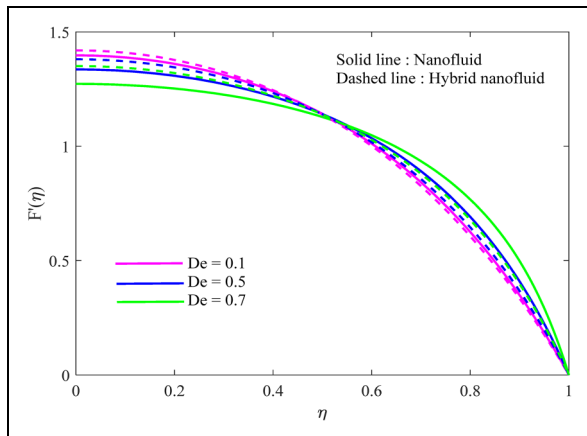


**Figure 3.** Velocity versus  $De$  for both nanofluid and hybrid nanofluid when  $Sq = 0.5$ ,  $\delta = 0.1$ ,  $Rd = 0.2$ ,  $Pr = 6.2$ ,  $\theta_w = 2$ , and  $Ec = 0.1$ .

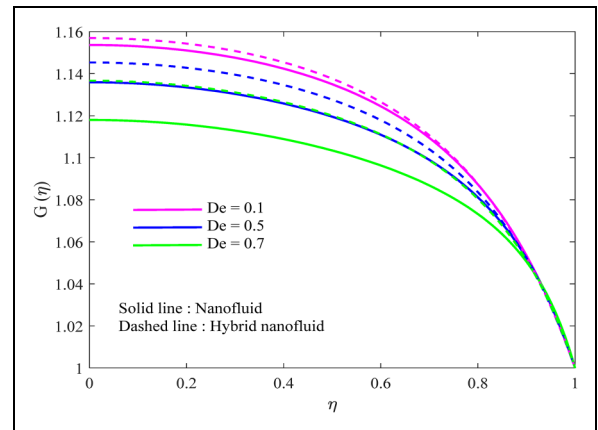


**Figure 6.** Temperature versus  $De$  for both nanofluid and hybrid nanofluid when  $Sq = 0.5$ ,  $\delta = 0.1$ ,  $Rd = 0.2$ ,  $Pr = 6.2$ ,  $\theta_w = 2$ , and  $Ec = 0.1$ .

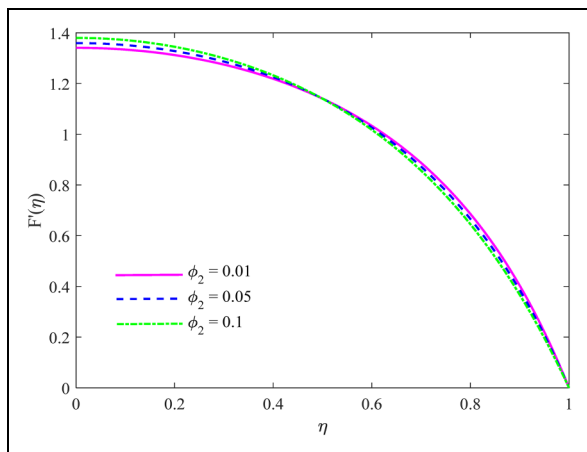


**Figure 4.** Velocity versus  $\phi_2$  for both nanofluid and hybrid nanofluid when  $De = 0.5$ ,  $Sq = 0.5$ ,  $\delta = 0.1$ ,  $Rd = 0.2$ ,  $Pr = 6.2$ ,  $\theta_w = 2$ , and  $Ec = 0.1$ .

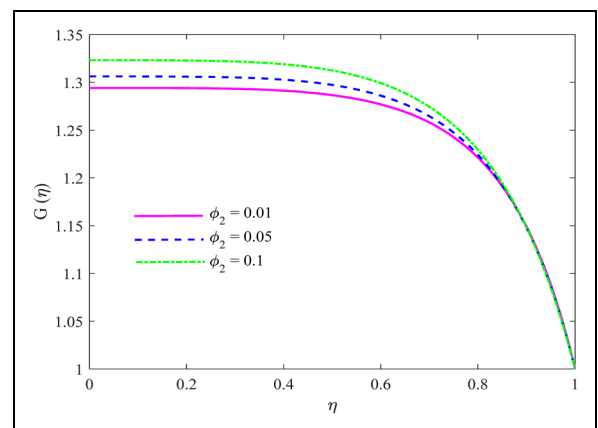


**Figure 7.** Temperature versus  $\phi_2$  for both nanofluid and hybrid nanofluid when  $De = 0.5$ ,  $Sq = 0.5$ ,  $\delta = 0.1$ ,  $Rd = 0.2$ ,  $Pr = 6.2$ ,  $\theta_w = 2$ , and  $Ec = 0.1$ .

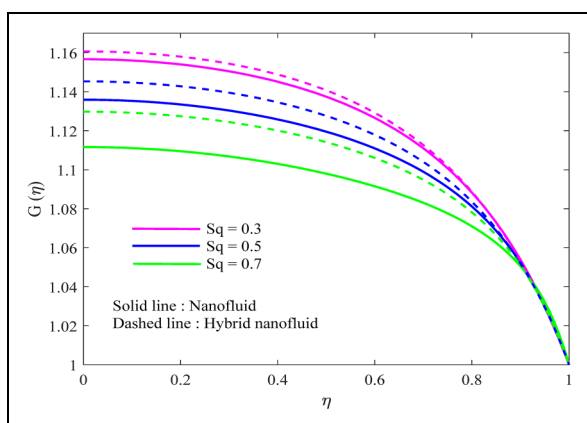


**Figure 5.** Temperature versus  $Sq$  for both nanofluid and hybrid nanofluid when  $De = 0.5$ ,  $\delta = 0.1$ ,  $Rd = 0.2$ ,  $Pr = 6.2$ ,  $\theta_w = 2$ , and  $Ec = 0.1$ .

Figures 5 to 10 give us an idea regarding the effect of various parameter values such as  $Sq$ ,  $De$ ,  $\phi_2$ ,  $Rd$ ,  $Ec$ , and  $\theta_w$  on thermal profiles within the squeezing

channel. Figure 5 exhibits the decrease in the thermal response for the positive values of  $Sq$  and for the negative values of  $Sq$ . We can observe an increase in the thermal response. The elastic properties of the Maxwell fluid likewise rise as  $Sq$  grows, whereas the thermal profile decreases. We also found that hybrid nanofluids have a higher thermal profile than nanofluids. Figure 6 illustrates that the higher values of  $De$  number minimise the temperature. Increasing the value of  $De$  will enhance the elastic property of Maxwell fluid; consequently, the heat transfer rate declines. Figure 7 exhibits that the thermal response slowly increases as the volume fraction of nanoparticles  $\phi_2$  increases. Supplementary Figure 8 exhibits that the thickness of the associated thermal boundary layer increases as a result of the thermal profile's growing relationship to the radiation parameter. The reason for this is that the Rosseland radiation absorptive diminishes as the radiation parameter rises. As a result, the absorption of Rosseland radiation declines, increasing the divergence of the radiative heat flux  $q_r$ . As a result, the fluid receives a rate of radiative heat transfer. It is the reason for the

**Table 3.** Numerical values for  $C_f$  and  $Nu$  for both nanofluid and hybrid nanofluid.

$Sq$	$De$	$Rd$	$\theta_w$	$Ec$	Nanofluid		Hybrid nanofluid	
					$C_f$	$Nu$	$C_f$	$Nu$
0.1	0.1	0.2	2	0.1	253.876	2.79496	330.86	3.64021
0.5					62.2271	2.82647	77.723	3.65169
1					38.2009	2.98421	45.8998	3.76810
2					27.4183	3.57402	30.4418	4.21812
	1				265.826	2.80145	341.529	3.64401
	2				267.502	2.82124	358.119	3.65435
	3				335.424	2.88665	384.388	3.67892
		0.4				2.80016		3.64537
		0.6				2.80244		3.64763
		0.8				2.80374		3.64892
		1.0				2.80457		3.64975
			3			2.80311		3.64829
			4			2.80596		3.65112
			5			2.80714		3.65228
				0.2		5.59248		7.28294
				0.3		8.39182		10.9275
				0.4		11.1925		14.5733
				0.5		13.9942		18.2201

increase in fluid temperature and the corresponding boundary-layer thickness. Supplementary Figure 9 shows that temperature increases with an increase in Eckert number  $Ec$ . From Supplementary Figure 10, we noticed that a rise in the temperature ratio parameter results in decrease in the thermal profile in the boundary-layer flow region.

Supplementary Figures 11 and 12 illustrate the impact of radiation parameter  $Rd$  and Eckert number  $Ec$  on the Bejan number  $Be$ . Supplementary Figure 11 displays the profile of  $Be$  number for radiation parameter  $Rd$ . Bejan number profile is declined for the increase of  $Rd$  as displayed in Supplementary Figure 11. As demonstrated in Supplementary Figure 12, the Bejan number profile is significantly increased for the Eckert number increments. In view of the fact that, the existence of Eckert number in a squeezing channel diminishes the thermal irreversibility. Supplementary Figures 13 and 14 expose the comparative study of  $E_{ST}$  and  $E_{SFF}$  for the variations of  $\phi_2$ . Entropy generation is high for the frictional forces when compared to thermal response as observed in Supplementary Figures 13 and 14. Moreover, both  $E_{ST}$  and  $E_{SFF}$  are increased for the increasing estimations of nanoparticles' volume fraction.

Table 3 gives us an idea regarding the results of skin friction  $C_f$  and Nusselt number  $Nu$  for the parameter of  $Sq$ ,  $De$ ,  $Rd$ ,  $\theta_w$  and  $Ec$ . For the rise in the squeezing parameter, it might be noted a decrease in skin friction values, whereas an increase in the Nusselt number. Increases in the physical parameters such as skin friction and Nusselt number follow increases in the  $De$  number. In addition, we can see the improvement in the Nusselt number for the increase in temperature ratio and radiation parameters. Final conclusion regarding physical parameters is that numerically these are high in hybrid nanofluid cases than that in nanofluid cases.

## 6. Conclusion remarks

By accounting for viscous dissipation and the impacts of radiative heat flux, the energy efficiency of the current analysis of squeezing flow of graphene-gold/PDMS hybrid Maxwell nanofluid between two plates is investigated numerically. The well-known Runge–Kutta–Fehlberg method is used to numerically solve the derived nonlinear differential equations. The following is a summary of some of the conclusions from the earlier analysis:

1. The number  $Be$  increases with the increasing radiation parameter  $Rd$ .
2. The  $Be$  number shows a downward trend with  $Ec$ .
3. Both  $E_{ST}$  and  $E_{SFF}$  increase with the increasing of the nanosize particle.
4. In squeezing channel, comparatively  $E_{SFF}$  is significantly greater than  $E_{ST}$ .
5. The velocity decreases to a certain range with increasing number of  $De$  number, the squeezing parameter, and then the trend is reversed.
6. With an increase in the radiation parameter  $Rd$  and the nanoparticle volume fraction  $\phi_2$ , the temperature inside the squeezing channel rises, but the squeezing parameter and the  $De$  number show the reverse trend.
7. Increases in the physical parameters such as skin friction and Nusselt number follow increases in the  $De$  number.
8. Skin friction values and the Nusselt number are higher for hybrid nanofluid than for nanofluid in this scenario.

## Acknowledgements

We are very grateful to the editor and reviewers for their constructive suggestions.


### Declaration of conflicting interests

The author(s) declared no potential conflicts of interest with respect to the research, authorship, and/or publication of this article.

### Funding

The author(s) received no financial support for the research, authorship, and/or publication of this article.

### ORCID iD

Kotha Gangadhar  <https://orcid.org/0000-0002-0264-2512>

### Supplemental material

Supplemental material for this article is available online.

### References

1. Stefan J. Versuche über die scheinbare adhesion. K. Akad. Wissenschaften. *Math. Naturwissenschaftliche Klasse, Wien, Sitzungsberichte* 1874; 69:713.
2. Siddiqui AM, Irum S and Ansari AR. Unsteady squeezing flow of a viscous MHD fluid between parallel plates, a solution using the homotopy perturbation method. *Math Model Anal* 2008; 13: 565–576.
3. Hayat T, Yousaf A, Mustafa M, et al. Influence of heat transfer in the squeezing flow between parallel disks. *Chem Eng Commun* 2012; 199: 1044–1062.
4. Vajravelu K, Prasad KV, Ng C-O, et al. MHD Squeeze flow and heat transfer of a nanofluid between parallel disks with variable fluid properties and transpiration. *Int J Mech Mater Eng* 2017; 12: 9.
5. Khan SI, Ahmed N, Khan U, et al. Heat transfer analysis for squeezing flow between parallel disks. *J Egypt Math Soc* 2015; 23: 445–450.
6. Mustafa M, Hayat T and Obaidat S. On heat and mass transfer in the unsteady squeezing flow between parallel plates. *Meccanica* 2012; 47: 1581–1589.
7. Bejan A. A study of entropy generation in fundamental convective heat transfer. *ASME J Heat Transf* 1979; 101: 718–725.
8. Bejan A. Second law analysis in heat transfer. *Energy* 1980; 5: 720–732.
9. Gul A, Khan I and Makhanov SS. Entropy generation in a mixed convection Poiseuille flow of molybdenum disulfide Jeffery nanofluid. *Results Phys* 2018; 9: 947–954.
10. Shit GC and Mukherjee S. MHD graphene-polydimethylsiloxane Maxwell nanofluid flow in a squeezing channel with thermal radiation effects. *Appl Math Mech -Eng Ed* 2019; 40: 1269–1284.
11. Marzougui S, Mebarek-Oudina F, Magherbi M, et al. Entropy generation and heat transfer of Cu-water nanofluid in porous lid-driven cavity through magnetic field. *Int J Numer Method H* 2022; 32: 2047–2069.
12. Sarbazi Z and Hormozi F. Numerical study of entropy generation and forced convection heat transfer of a nanofluid in a channel with different fin cross-sections. *Int J Numer Method H* 2022; 32: 62–98.
13. Mehta SK, Pati S, Ahmed S, et al. Analysis of thermo-hydraulic and entropy generation characteristics for flow through ribbed-wavy channel. *Int J Numer Method H* 2022; 32: 1618–1642.
14. Abbasi FM, Gul M, Shanakhat I, et al. Entropy generation analysis for magnetized peristaltic movement of nanofluid through a non-uniform asymmetric channel with variable thermal conductivity. *Chin J Phys* 2022; 78: 111–131.
15. Zheng Y, Yaghoubi S, Dezfulezadeh A, et al. Free convection/radiation and entropy generation analyses for nanofluid of inclined square enclosure with uniform magnetic field. *J Therm Anal Calorim* 2020; 141: 635–648.
16. Boland CS, Khan U, Ryan G, et al. Sensitive electromechanical sensors using viscoelastic graphene-polymer nanocomposites. *Science* 2016; 354: 1257–1260.
17. Choi SU and Eastman JA. Enhancing Thermal Conductivity of Fluids with Nanoparticles. *Argonne National Lab., IL (United States)* 1995.
18. Acharya N, Das K and Kundu PK. The squeezing flow of Cu-water and Cu-kerosene nanofluids between two parallel plates. *Alex Eng J* 2016; 55: 1177–1186.
19. Pourmehran O, Rahimi-Gorji M, Gorji-Bandpy M, et al. Analytical investigation of squeezing unsteady nanofluid flow between parallel plates by LSM and CM. *Alex Eng J* 2015; 54: 17–26.
20. Subhani M and Nadeem S. Numerical analysis of 3D micropolar nanofluid flow induced by an exponentially stretching surface embedded in a porous medium. *Eur Phys J Plus* 2017; 132: 441.
21. Nadeem S, Abbas N and Khan AU. Characteristics of three dimensional stagnation point flow of Hybrid nanofluid past a circular cylinder. *Results Phys* 2018; 8: 829–835.
22. Gangadhar K, Keziya K and Ibrahim SM. Effect of thermal radiation on engine oil nanofluid flow over a permeable wedge under convective heating Keller box method. *Multidiscip Model Mater Struct* 2019; 15: 187–205.
23. Butt AS, Ali A, Masood R, et al. Parametric study of entropy generation effects in magneto hydrodynamic radiative flow of second grade nanofluid past a linearly convective stretching surface embedded in a porous medium. *J Nanofluids* 2018; 7: 1004–1023.
24. Afridi MI and Qasim M. Comparative study and entropy generation analysis of CU-H<sub>2</sub>O and AG-H<sub>2</sub>O nanofluids flow over a slandering stretching surface. *J Nanofluids* 2018; 7: 783–790.
25. Saleem S, Qasim M, Alderremy A, et al. Heat transfer enhancement using different shapes of Cu nanoparticles in the flow of water based nanofluid. *Phys Scr* 2020; 95: 055209.
26. Shah Z, Dawar A, Kumam P, et al. Impact of nonlinear thermal radiation on MHD nanofluid thin film flow over a horizontally rotating disk. *Appl Sci* 2019; 9: 1533.
27. Shahzadi I, Suleman S, et al. Utilization of Cu-nanoparticles as medication agent to reduce atherosclerotic lesions of a bifurcated artery having compliant walls. *Comput Methods Programs Biomed* 2020; 184: 105123.
28. Belhaj S and Ben-Beya B. Thermal performance analysis of hybrid nanofluid natural convection in a square cavity containing an elliptical obstacle under variable magnetic field. *Int J Numer Method H* 2022; 32: 1825–1860.
29. Nemati M, Sani HM, Jahangiri R, et al. MHD Natural convection in a cavity with different geometries filled with a nanofluid in the presence of heat generation/absorption using little Boltzmann method. *J Therm Anal Calorim* 2022; 147: 9067–9081.
30. Pathak AK, Tyagi VV, Anand S, et al. Advancement in solar still integration with phase change materials-based TES systems and nanofluid for water and wastewater

- treatment applications. *J Therm Anal Calorim* 2022; 147: 9181–9227.
31. Shami S, Sajid M and Javed T. Analysis of heat transfer in SWCNTs-ethylene glycol-based nanofluid past a vertical complex wavy surface. *J Therm Anal Calorim* 2022; 147: 2601–2613.
  32. Wahid NS, Arifin NM, Khashiie NS, et al. Hybrid nanofluid stagnation point flow past a slip shrinking Riga plate. *Chin J Phys* 2022; 78: 180–193.
  33. Kausar MS, Hussanan A, Waqas M, et al. Boundary layer flow of micropolar nanofluid towards a permeable stretching sheet in the presence of porous medium with thermal radiation and viscous dissipation. *Chin J Phys* 2022; 78: 435–452.
  34. Subramanian R, Senthil Kumar A, Vinayagar K, et al. Experimental analyses on heat transfer performance of TiO<sub>2</sub>water nanofluid in double-pipe counter-flow heat exchanger for various flow regimes. *J Therm Anal Calorim* 2020; 140: 603–612.
  35. Khan SA, Hayat T, Alsaedi A, et al. Melting heat transportation in radiative flow of nanomaterials with irreversibility analysis. *Renew Sust Energy Rev* 2021; 140: 110739.
  36. Hayat T, Khan SA and Alsaedi A. Irreversibility characterization in nanoliquid flow with velocity slip and dissipation by a stretchable cylinder. *Alex Eng J* 2021; 60: 2835–2844.
  37. Khan SA, Hayat T and Alsaedi A. Entropy optimization in passive and active flow of liquid hydrogen based nanoliquid transport by a curved stretching sheet. *Int Commun Heat Mass Transf* 2020; 119: 104890.
  38. Hayat T, Khan SA, Alsaedi A, et al. Computational analysis of heat transfer in mixed convective flow of CNTs with entropy optimization by a curved stretching sheet. *Int Commun Heat Mass Transf* 2020; 118: 104881.
  39. Khan SA, Hayat T, Ijaz Khan M, et al. Salient features of Dufour and Soret effect in radiative MHD flow of viscous fluid by a rotating cone with entropy generation. *Int J Hydrog Energy* 2020; 45: 14552–14564.
  40. Khan SA, Saeed T, Ijaz Khan M, et al. Entropy optimized CNTs based Darcy-Forchheimer nanomaterial flow between two stretchable rotating disks. *Int J Hydrog Energy* 2019; 44: 31579–31592.
  41. Hayat T, Khan SA, Ijaz Khan M, et al. Theoretical investigation of Ree–Eyring nanofluid flow with entropy optimization and Arrhenius activation energy between two rotating disks. *Comput Methods Programs Biomed* 2019; 177: 57–68.
  42. Hayat T, Khan SA and Alsaedi A. Simulation and modeling of entropy optimized MHD flow of second grade fluid

with dissipation effect. *J Mater Res Technol* 2020; 9: 11993–12006.

## Nomenclature

### Roman letters

$t$	time (s)
$f_1, f_2$	velocity components (ms <sup>-1</sup> )
$T$	temperature (K)
$p$	pressure (Pa)
$k$	thermal conductivity (W m <sup>-1</sup> K <sup>-1</sup> )
$q_r$	heat flux (W m <sup>-2</sup> )
$k_0$	mean absorption coefficient (m <sup>-1</sup> )
$T_H$	ambient temperature (K)
$T_w$	wall temperature (K)
$Sq$	squeezing parameter
$Ec$	Eckert number
$Pr$	Prandtl number
$De$	Deborah number
$Rd$	radiation parameter
$C_f$	skin friction coefficient
$Nu$	Nusselt number
$F'$	dimensionless velocity
$G$	dimensionless temperature

### Greek symbols

$\phi$	nanoparticle volume fraction
$\sigma_0$	Stefan–Boltzmann constant (W m <sup>-2</sup> K <sup>-4</sup> )
$\rho C_p$	heat capacity (J kg <sup>-1</sup> K <sup>-1</sup> )
$\rho$	density (kg m <sup>-3</sup> )
$\mu$	dynamic viscosity (kg m <sup>-1</sup> s <sup>-1</sup> )
$\xi_1, \xi_2$	Cartesian coordinates (m)
$\lambda_1$	relaxation time

### Subscripts

$f$	base fluid
$nf$	nanofluid
$hnf$	hybrid nanofluid
$s_1$	solid component for gold
$s_2$	solid component for graphene